CMS Physics Analysis Summary

Contact: cms-pog-conveners-muons@cern.ch 2010/07/21

Performance of muon identification in pp collisions at $\sqrt{s} = 7$ TeV

The CMS Collaboration

Abstract

The performance of muon identification in CMS has been studied on a sample of muons corresponding to an integrated luminosity of up to 84 nb^{-1} collected in pp collisions at $\sqrt{s} = 7$ TeV at the LHC. Measured distributions of basic muon-track quantities are well reproduced by the Monte Carlo simulation. Efficiencies of various high-level trigger, identification, and reconstruction algorithms have been measured in the muon momentum range up to about 15 GeV/c, and found to agree typically within 5-10% of expectations. The probability to mis-identify kaons or pions as muons due to their decay in-flight agrees with predictions from simulation. The punch-through probability for protons with momentum between 3 and 10 GeV/c was measured to be $(5.3 \pm 0.8\ (\text{stat.})) \cdot 10^{-4}$, in agreement with expectations.

1 Introduction

Many of the rare physics processes searched for in hadron collider events are characterized by leptons in the final state. Leptons provide a striking signature in a large background of jets, allowing for the identification of rare signal events. This is especially true for muons. Thus it is crucial for CMS [1] to be able to detect muons with high efficiency, low fake-rate from backgrounds, and excellent momentum resolution.

Muon reconstruction in CMS and the response of various subdetectors to muons have been studied in great detail using muons from cosmic rays [2, 3]. In this note we report for the first time on the performance of the CMS muon reconstruction and trigger in proton-proton collision data.

In the first four months of LHC [4] operation at $\sqrt{s}$ = 7 TeV, CMS has recorded more than 200 nb^{-1} of proton-proton collision data. Results presented in the following are obtained using data samples corresponding to an integrated luminosity between 0.47 nb^{-1} (for studies requiring a minimum bias trigger) and 84 nb^{-1} (for studies that can use data samples collected with a muon trigger).

The muon momentum scale is known with a relative accuracy of 0.1% up to 10 GeV/c and 0.5% up to 100 GeV/c [5]. For transverse momentum below 10 GeV/c the relative momentum resolution is around 1% (2%) in the barrel (endcap) [5].

2 Muon Reconstruction and Identification in CMS

Muon tracking in CMS is performed with the all-silicon tracker at the heart of the detector, and with up to four stations of gas-ionization muon detectors [6] installed outside the solenoid, sandwiched between steel layers serving both as hadron absorbers and as a return yoke for the magnetic field. Drift Tube (DT) chambers and Cathode Strip Chambers (CSC) are used in the barrel ($|\eta|$ <1.2) and endcaps (0.9< $|\eta|$ <2.4) respectively, complemented by a system of Resistive Plate Chambers (RPC) covering both regions (up to $|\eta| < 1.6$). A cross-section of CMS is shown in Fig. 1. Muon energy deposits in the electromagnetic calorimeter (ECAL), hadronic calorimeter (HCAL) and outer hadronic calorimeter (HO) are also used for muon identification purposes (see Section 4). A detailed description of CMS can be found elsewhere [1].

The CMS experiment uses a two-level trigger system. The first level is hardware-based and is called the "Level-1 Trigger" (L1) while the second level is software-based and is called the "High-Level Trigger" (HLT) [7]. The muon trigger is discussed further in Section 7.

In the standard CMS reconstruction for pp collisions [3, 8], tracks are first reconstructed independently in the silicon tracker (*tracker track*) and in the muon spectrometer (*standalone-muon track*). Based on these, two reconstruction approaches are used:

1. *Global Muon reconstruction (outside-in):* starting from a standalone muon in the muon system, a matching tracker track is found and a *global-muon track* is fitted combining hits from the tracker track and standalone-muon track. At large transverse momenta ($p_{\mathrm{T}} \gtrsim 200$ GeV/c), the global-muon fit can improve the momentum resolution compared to the tracker-only fit [3, 8].

2. *Tracker Muon reconstruction (inside-out):* in this approach, all tracker tracks with $p_{\mathrm{T}} >$ 0.5 GeV/c and $p >$ 2.5 GeV/c are considered as possible muon candidates and are extrapolated to the muon system, taking into account the expected energy loss and the

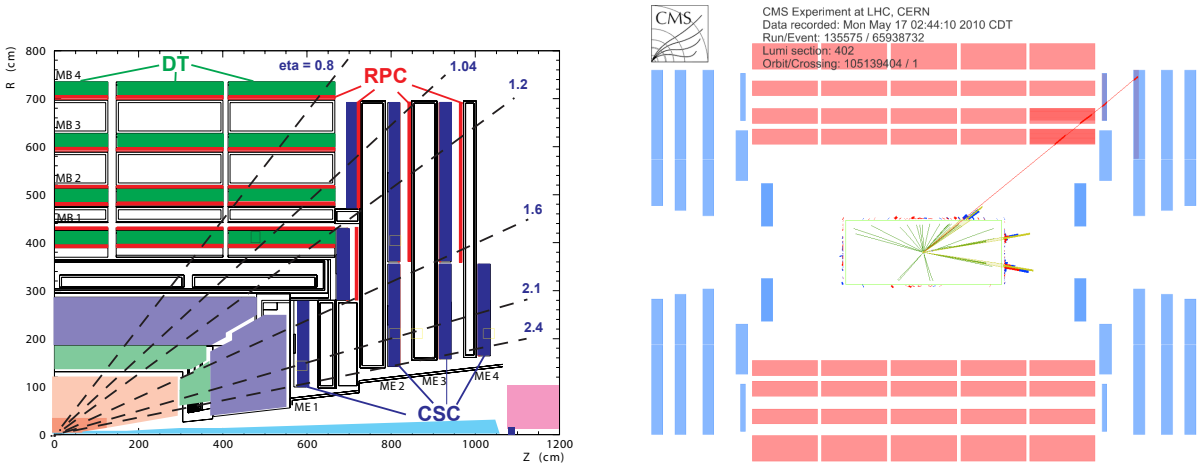

Figure 1: Layout of one quadrant of CMS (left), and a display of a collision event with a muon crossing the DT and CSC chambers in the overlap region between barrel and endcap (right).

uncertainty due to multiple scattering. If at least one muon segment (i.e. a short track stub made of DT or CSC hits) matches the extrapolated track in position, the corresponding tracker track qualifies as a *tracker-muon track*.
At low momentum (roughly $p < 5$ GeV/c) this approach is more efficient than the global muon reconstruction, since it requires only a single muon segment in the muon system, while global muon reconstruction typically becomes efficient with two or more segments.

The majority of muons from collisions (with sufficient momentum) are reconstructed either as a Global Muon or a Tracker Muon, or very often as both. However, if both approaches fail and only a *standalone-muon track* is found, this leads to a third category of muon candidates:

3. *Standalone-muon track only*: this occurs only for about 1% of muons from collisions, thanks to the high tracker-track efficiency [9]. On the other hand, the acceptance of this type of muon track for cosmic-ray muons is a factor 10^2 to 10^3 larger, thus leading to a collision muon to cosmic-ray muon ratio that is a factor 10^4 to 10^5 less favourable than for the previous two muon categories.

The results of these three algorithms are merged into a single collection of muon candidates, each one containing information from the standalone, tracker, and global fit, when available. Candidates found both by the Tracker Muon and the Global Muon approach that share the same tracker track are merged into a single candidate. Similarly, standalone-muon tracks not included in a Global Muon are merged with a Tracker Muon if they share a muon segment. Additional muon identification information (cf. Section 4) is stored for each candidate.

The combination of different algorithms provides a robust and efficient muon reconstruction. A given physics analysis can achieve the desired balance between identification efficiency and purity by applying a selection based on the muon identification variables. Several standard selections are provided. In this note we study the performance of three basic selections:

- *Soft Muon Selection:* This selection requires the candidate to be a Tracker Muon, with the additional requirement that a matching segment be found in the outermost station where a segment is expected (based on muon position and momentum), matching both in position and direction with the prediction of the track extrapolation.

Segments that form a better match in position with a different tracker track are not considered. These additional requirements are optimized for low p_{T} (< 10 GeV/c) muons. This selection is presently used in B-physics analyses in CMS [10], in addition to Global Muons.

- *Global Muon Selection:* Here the only requirement is that the candidate be a Global Muon.
- *Tight Muon Selection:* For this selection, the candidate must be reconstructed both inside-out as a Tracker Muon and outside-in as a Global Muon, with the following additional requirements: $p_T > 3$ GeV/c; normalized χ^2 of the global-muon track fit < 10; at least one muon chamber hit included in the final track fit; matched to muon segments in at least two muon stations; and its corresponding tracker track must have more than 10 silicon tracker hits (including at least one pixel hit) and a transverse impact parameter $|d_{xy}| < 2$ mm with respect to the primary vertex. With this selection, the rate of muons from decays-in-flight is significantly reduced (cf. Section 3), at the price of a few percent loss in efficiency for prompt muons such as those from Z and W decays (cf. Section 5). The muon selection presently used in CMS electroweak analyses [11] includes requirements similar to this 'Tight Muon' selection.

A display of an event containing a reconstructed muon passing all the above selections is shown in Fig. 1. More event displays are included in the Appendix.

3 Kinematic Distributions

In this section we present kinematic distributions of a fully inclusive sample of muons reconstructed in minimum-bias collision events. The data sample contains 23.1 million events, corresponding to 0.47 nb^{-1} of integrated luminosity recorded with a minimum bias trigger and requiring a reconstructed primary vertex in the event. The integrated luminosity is small because the minimum bias trigger was unprescaled only at the beginning of data taking (a prescale factor of 500 or more is typical at current luminosities). For the simulation we use about 54 million minimum bias events generated with PYTHIA 6.422 with the D6T tune [12] (corresponding to about 0.76 nb^{-1} of integrated luminosity). The presence of a reconstructed primary vertex is requested in simulation as well; this requirement is found to be 99% efficient for simulated events having at least one reconstructed muon.

The simulation is normalized according to the integrated luminosity of the data sample estimated using the observed fraction of zero-bias events without a reconstructed vertex (the so-called Offline Vertex Method [13]). The uncertainty in the absolute value of luminosity is currently estimated to be 11% [13]. As part of this uncertainty is not relevant for the relative normalization we use (based on requiring one reconstructed track vertex in both detected and simulated minimum bias events), this way of normalizing simulation to data has a precision better than 11%.

The number of muons per event in the inclusive minimum bias sample is shown in Fig. 2, for Soft Muons, Global Muons, and Tight Muons. The fractions of events with at least one reconstructed muon are 1.0%, 0.20% and 0.04% for these three muon selections, respectively. The agreement between data and simulation is good.

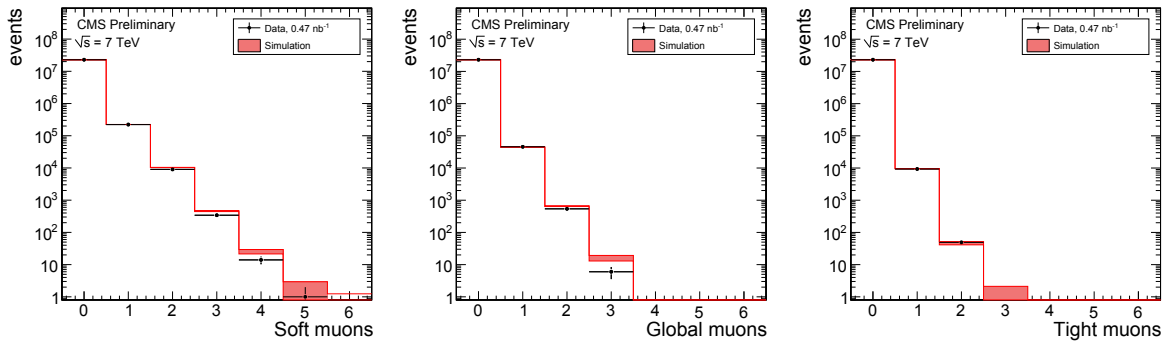

Figure 2: The number of Soft Muons (left), Global Muons (center), and Tight Muons (right) per event, in a sample of 23.1 million minimum bias events.

3.1 Classification of muon sources in simulation

For each reconstructed muon in simulation, the hits in the muon system are matched unambiguously to the simulated particle that produced them. This allows the classification of reconstructed muons into the following categories:

- *Muons from heavy flavour:* Here the majority of muon chamber hits associated to the muon candidate were produced by a true muon. The muon's parent particle can be a beauty meson, charmed meson, tau lepton or any other particle (like W or Z) not included in the "Light Flavour" category.
- *Muons from light flavour:* In this category, the majority of muon chamber hits of the muon candidate were produced by a true muon. This muon originated from light hadron decays (π and K) or, less frequently, from a calorimeter shower or a product of a nuclear interaction in the detector.
- *Hadron punch-through:* Here the majority of muon chamber hits of the muon candidate were produced by a particle other than a muon. The so-called "punch-through" is the source of the majority of these candidates ($\sim$ 88% for Global Muons) although "sail-through" (i.e. without any interaction before the muon system) is present as well.
- *Duplicate:* If one simulated particle gives rise to more than one reconstructed muon candidate, the one with the largest number of matched hits is flagged according to one of the other categories. Any others are labeled as "duplicate". These are duplicate candidates created by instrumental effects or imperfections in the pattern recognition of the reconstruction software.

3.2 Results

In Fig. 3, distributions are shown for Tight Muons of the transverse momentum p_{T}, pseudo-rapidity η and azimuthal angle ϕ. Similar plots for Soft Muons and Global Muons are presented in Ref. [14]. The pseudo-rapidity distribution peaks in the forward region because there the minimum p_{T} required to reach muon stations is lower than in the barrel; in that region the threshold in p_{T} is about 3-4 GeV/c, while in the endcaps it is about 0.5 GeV/c. In general the agreement between data and predictions from the simulation is good over the whole accessible range.

Table 1 lists the sources of muons according to simulation for reconstructed muons in minimum-bias events. The majority of reconstructed muon candidates originate from decays-in-

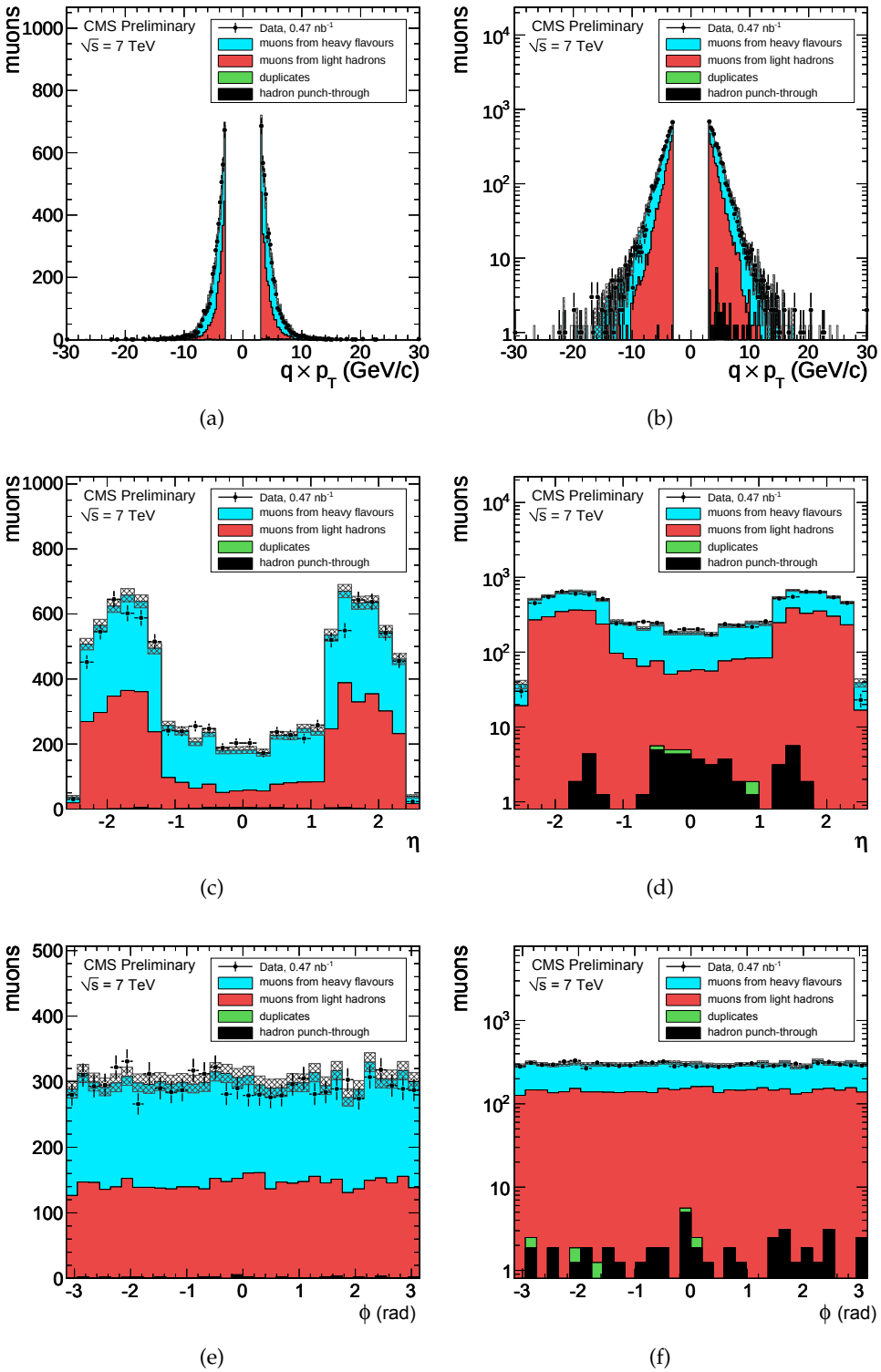

Figure 3: Distributions of kinematic variables for Tight Muons, comparing data (points with error bars) to minimum-bias simulation, which is separated into its different components. The kinematic variables are the transverse momentum (top) for positively- and negatively-charged muons, pseudo-rapidity (center) and azimuthal angle (bottom), shown in linear (left) and logarithmic scale (right). The error bars (for data points) and grey boxes (for simulation) indicate the statistical uncertainty.

flight of pions and kaons ("light flavour"). At higher momentum the contribution of muons from heavy flavour decays increases. The rate of punch-through and fake muons is about 7% for Soft Muons and 2% for Global Muons even without any muon quality selections, according to the Monte Carlo simulation. For Tight Muons the fraction is even smaller at 0.5%, and the simulation predicts that the majority of this punch-through is from K^+, leading to the charge asymmetry visible in the punch-through component in Fig. 3(b). Data-driven measurements presented in Section 5.2 confirm that the simulation correctly estimates the probability for light-flavour decays to be identified as muons. A comparison of the overall event yield in data and simulation is shown in Table 2. The uncertainty quoted on the prediction from simulation only includes the statistical uncertainty. The systematic uncertainty on the simulated yield due to the normalization according to luminosity [13] and the modeling by PYTHIA of QCD effects in minimum bias events is significantly larger than the statistical uncertainty quoted.

Table 1: Composition of the sources of reconstructed muons in minimum bias events according to simulation for different muon selections.

muon source [%]	Soft Muon	Global Muon	Tight Muon
heavy flavour	8.83	23.9	52.0
light flavour	83.9	73.6	47.5
duplicate	2.82	0.65	0.03
hadron punch-through	4.44	1.84	0.49

Table 2: Comparison of event yield in data and simulation (normalized to the same integrated luminosity of the data sample) for different muon selections. The quoted uncertainties are statistical only.

overall yield [no. of muons]	Soft Muon	Global Muon	Tight Muon
data	241 381	46 742	9 435
simulation $\times 10^3$	245.7 ± 0.4	46.12 ± 0.17	9.66 ± 0.08
ratio data/simulation	0.982 ± 0.002	1.014 ± 0.006	0.977 ± 0.013

4 Muon Identification Variables

The standard CMS reconstruction provides additional information for each muon, useful for muon quality selection and identification (ID) in physics analyses.

Track quality information includes the number of hits associated to the tracker track, standalone-muon track and global-muon track, the χ^2 of the various fits, the number of "good" hits (those having small residual with respect to the track), and the number of layers where a hit would be expected but no hit was found. A comparison between data and simulation for a selection of these variables is shown in Fig. 4, using the same minimum bias data and simulated samples used in Section 3. The average number of hits on global tracks is lower than expected by about 5%. This difference is not in the number of silicon tracker hits, but is due to a smaller number of associated muon hits. This is believed to be related to calibration and alignment conditions at start-up. Distributions of the transverse impact parameter of the muon with respect to the primary vertex and its significance are well reproduced by the simulation.

Other muon ID information includes matching information for segments in the different stations of the muon system matched to the tracker track extrapolation, with residuals in position and direction and their corresponding uncertainties. Compatibility variables (having a value

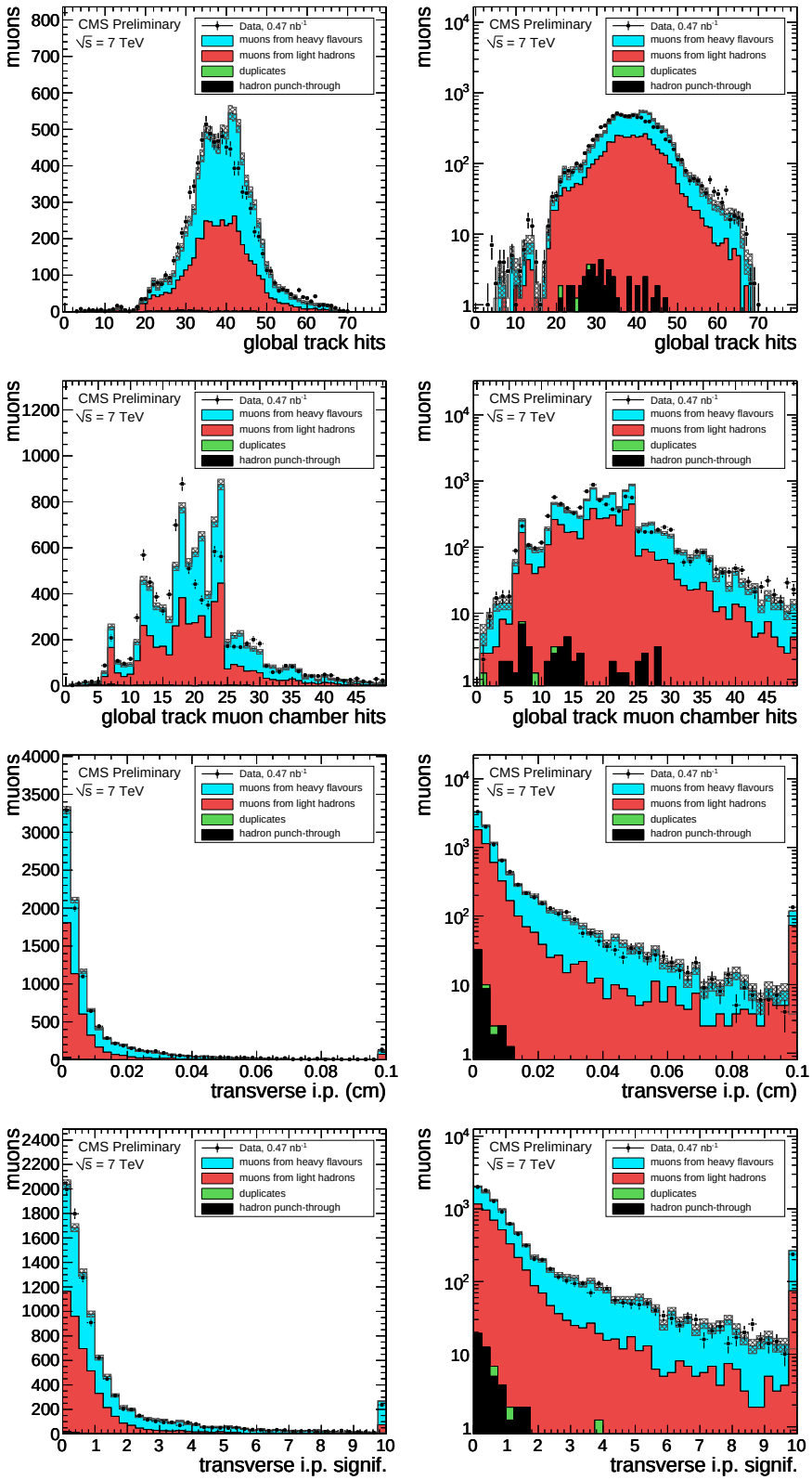

Figure 4: Tracking variables for Tight Muons, in linear scale (left) and logarithmic scale (right). From top to bottom: the number of hits on the global track (including hits in silicon tracker and the muon system); the number of muon chamber hits on the global track; the transverse impact parameter; and significance of the transverse impact parameter. The error bars (for data points) and grey boxes (for simulation) indicate the statistical uncertainty.

between 0 and 1) are provided based on muon segment information, giving the most weight to muon segments in the outer layers of the muon system (the "muon segment compatibility") and based on the matched energy deposits in the calorimeters (the "calorimeter compatibility") [3, 8].

5 Muon Identification Efficiency for Signal and Backgrounds

The previous sections focused on the comparison between data and simulation for inclusive distributions of relevant muon reconstruction and identification variables. In this section we study exclusive samples of prompt muons, kaons, pions and protons in data to determine the probability for these particles to be reconstructed as a muon.

5.1 Muon efficiency using the tag-and-probe method on the J/ψ resonance

5.1.1 Method

We evaluate the efficiencies for low-momentum prompt muons by applying a "tag-and-probe" technique to muons from the $J/\psi \to \mu\mu$ resonance. Using this technique it is possible to obtain almost-unbiased estimates of the efficiencies of the different stages of muon trigger and offline reconstruction. Events are selected with strict selection requirements on one muon (the 'tag' muon), and with a more relaxed selection on the other muon (the 'probe' muon), such that the selection applied to the probe muon does not bias the efficiency that one wants to measure. The fraction of probe muons which passes the selection under study gives an estimate of its efficiency.

In the case of the $J/\psi \to \mu\mu$ events, combinatorial backgrounds from other tracks in the event are generally high. A powerful way to reduce this background further is to require that the candidate probe muon has the signature of a minimum-ionizing particle (MIP) in the calorimeter. By requiring a calorimeter compatibility (Section 4) above 0.6, the background can be reduced by about a factor of three without using any information from the muon system. In Fig. 5(a) we show an example of the dimuon invariant mass spectrum in one of the most challenging $\eta - p_T$ bins, illustrating the effect of applying such MIP requirement.

Still the background remains large, so it is important to subtract it. For this purpose, we use the di-muon invariant mass spectrum in the mass window from 2.8 to 3.5 GeV/c^2. Figures 5(b) and (c) show an example of background subtraction in the determination of the Soft Muon reconstruction efficiency given that a tracker track exists, applied to a data sample corresponding to 60 nb^{-1}. In this case the tag muon is a Global Muon, and the probe muon is a tracker track with MIP signature. The passing criterion is whether the tracker track is identified as a Soft Muon. The invariant mass spectra for passing and failing probes are fitted with identical signal shape and appropriate background shapes. The two fits give one measured point in the efficiency plot in Fig.5(b), in this case for probe muons with a p_T between 0 and 2 GeV/c and $|\eta| > 1.2$. Run on simulation, the tag-and-probe results agree well with the "simulation truth", defined as the efficiency for probes *that are true signal muons* to satisfy the passing criterion, confirming that background subtraction is adequate.

5.1.2 Results

Figure 6 shows the muon reconstruction efficiency given that a tracker track exists. The tag is defined as a Global Muon that passed the single-muon trigger, and the probe is a tracker track with MIP signature and $p_T > 2$ GeV/c for $|\eta| < 1$ or $p > 2$ GeV/c for $|\eta| > 1$. The simulation sample corresponds to more than 200 nb^{-1} of integrated luminosity and includes backgrounds;

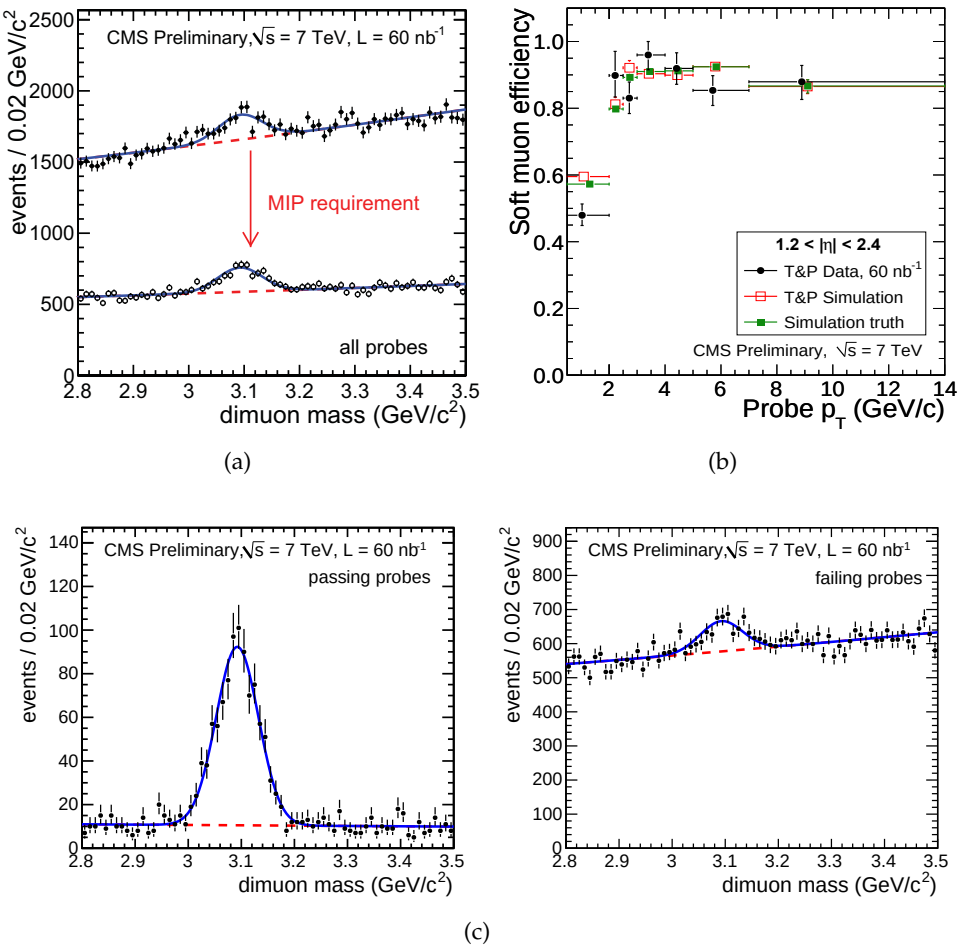

Figure 5: Example of background subtraction to determine the Soft Muon ID efficiency for $0 < p_{\mathrm{T}} < 2$ GeV/c and $1.2 < |\eta| < 2.4$, given that the tracker track exists. a) shows the reduction of the background (for all probes) using the MIP requirement. c) these two plots show the lineshapes for passing and failing probes. Background subtraction is applied, to produce the 1$^{\mathrm{st}}$ bin in plot b), where the tag-and-probe efficiencies as a function of p_{T} in the endcaps ($1.2 < |\eta| < 2.4$) in data and in simulation are compared to the efficiency with perfectly subtracted background (the "Simulation truth") in simulation.

the data sample corresponds to 84 nb^{-1}. The tag-and-probe results in simulation and data agree rather well, within about 5-10% (absolute difference in efficiency). The most significant deviation is a higher-than-expected efficiency in data in the barrel, between 3 and 7 GeV/c, by about 5-10%. This is visible in the Soft Muon and Tight Muon efficiency, but much less so in the Global Muon plots. As expected, the Soft Muon selection has a higher efficiency than Global and Tight Muons at low p_{T}, while for a p_{T} above about 5 GeV/c, the efficiency plateau is lower than for Global or Tight Muons. This is because the Soft Muon selection, by design, has strict requirements on the outermost muon segment; these requirements are suitable to enhance the purity in the low momentum region but are superfluous at higher values of p_{T}.

The tag-and-probe measurements for the same types of efficiencies have also been made without the requirement that the probe tracks have a MIP signature. The results are fully compatible within slightly larger statistical uncertainties. Simulation studies show that in this low

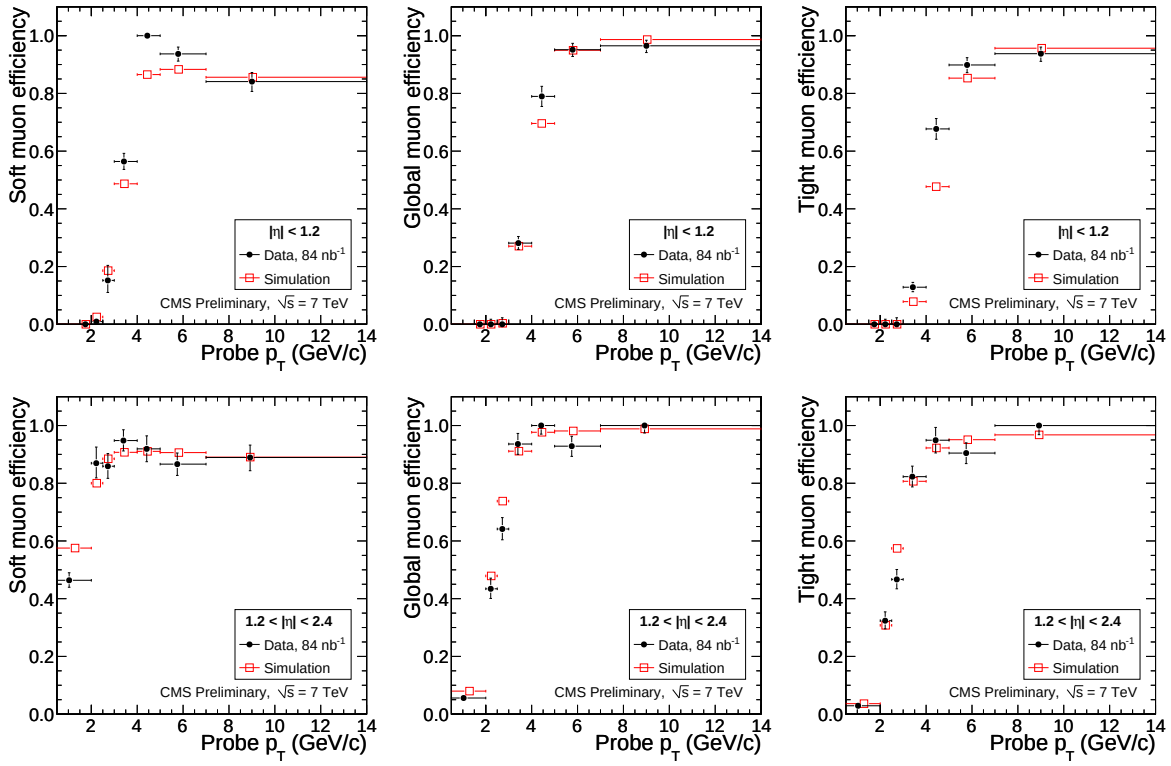

Figure 6: Tag-and-probe results for the muon reconstruction efficiency in data compared to simulation. Given that a tracker track exists (with a MIP signature), the plots show the efficiency as a function of muon p_{T} for Soft Muons (left), Global Muons (middle) and Tight Muons (right) in the barrel (top) and endcaps (bottom).

p_{T} range, tag-and-probe efficiencies estimated with a MIP requirement are systematically 1-2% higher than without a MIP requirement (absolute difference in efficiency). This effect is expected to cancel to first order in the data/simulation ratio.

Using the same technique, it is possible to measure the efficiency for the muon track in the silicon tracker to be reconstructed. In this case a standalone-muon track is used as a probe. Due to the worse resolution for standalone-muon tracks, the mass peak is broader, but the background is small. The invariant mass distribution and efficiency results are reported elsewhere [9] and show that for muons of sufficient momentum to create a standalone muon, the efficiency is 99% or higher in the entire acceptance $|\eta| < 2.4$ both in data and in simulation.

In Section 7, tag-and-probe results are shown for the trigger efficiency.

5.2 Muon identification probability for particles other than muons

One can obtain pure samples of kaons, pions, and protons from resonances of particle decays such as $\mathrm{K_S}^0 \to \pi^+\pi^-$, $\Lambda \to p\pi^-$(and charge conjugate), and $\phi \to \mathrm{K}^+\mathrm{K}^-$. The resonances are reconstructed using pairs of tracker tracks that match to a common decay vertex, with a selection similar to the one described in Ref. [15]. In Λ decays, the highest momentum track is assumed to be the proton. A data sample collected with a minimum bias trigger is used.

We then compute the fraction of events in which these tracks are identified as a Soft Muon, Global Muon or Tight Muon as a function of several relevant track parameters. Bin-by-bin background subtraction is performed to determine the muon identification probability for the

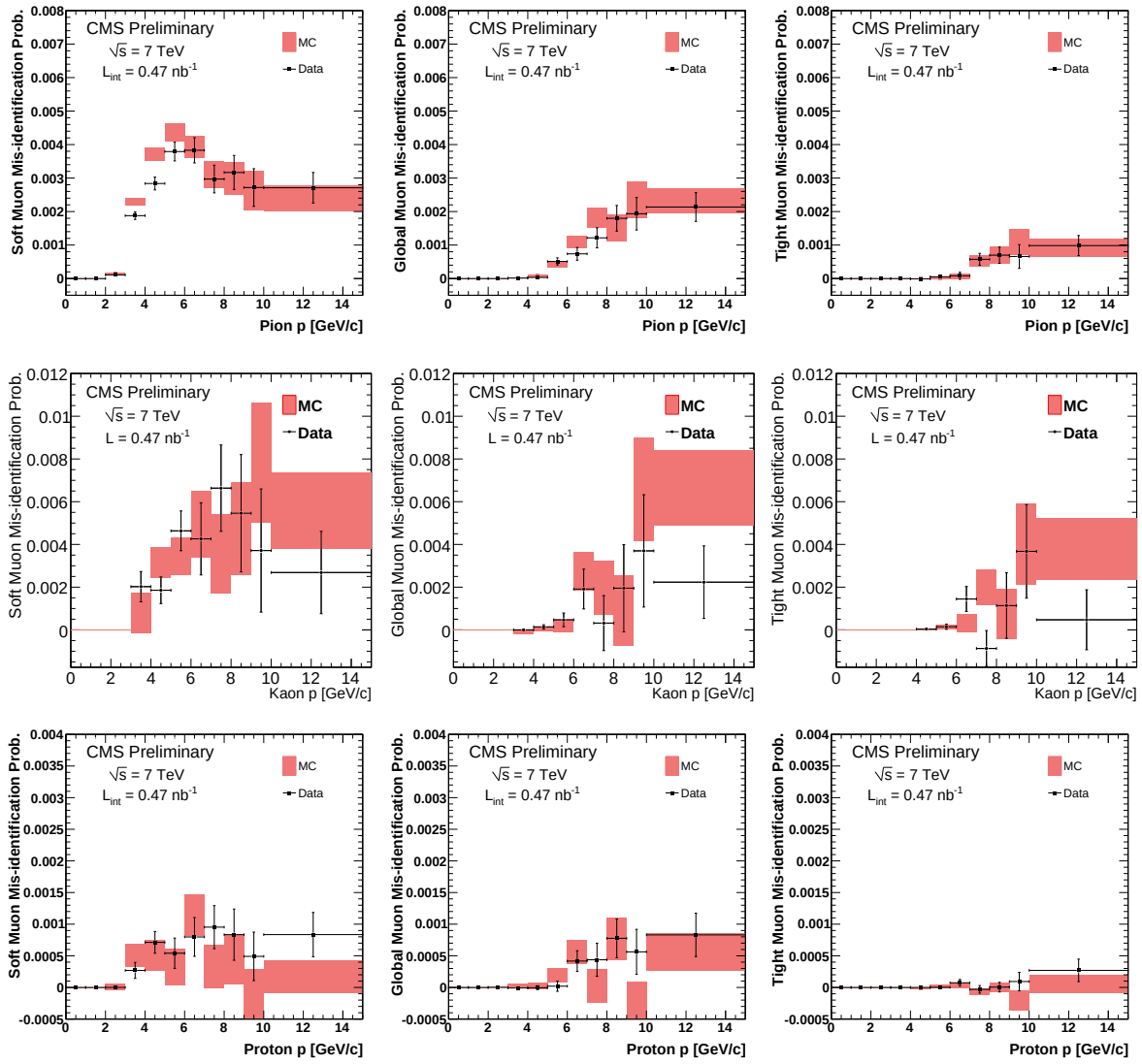

Figure 7: The fraction of pions (top), kaons (center) or protons (bottom) that are mis-identified as a Soft Muon (left), Global Muon (center) or Tight Muon (right) as a function of momentum. The uncertainties indicated by the error bars (data) and grey boxes (PYTHIA simulation) are statistical only.

particles under study. The same method is applied to data and minimum-bias simulated events.

The resulting muon mis-identification probabilities as a function of particle momentum and pseudo-rapidity are shown in Figs. 7 and 8. As expected, these probabilities are found to be independent, within statistical uncertainty, of the azimuthal angle and the decay length of the mother particle. An interesting structure, well reproduced by simulation, is observed as a function of pseudo-rapidity and momentum. It is due to a combination of acceptance (a minimum momentum is required to reach the muon system), the amount of material before the muon system, and the distance available for pions and kaons to decay before reaching the calorimeter. At very low p_{T} the muon mis-identification probability is lower for Global Muons than for Soft Muons, while for a momentum of about 10 GeV/c they are similar. The reason for

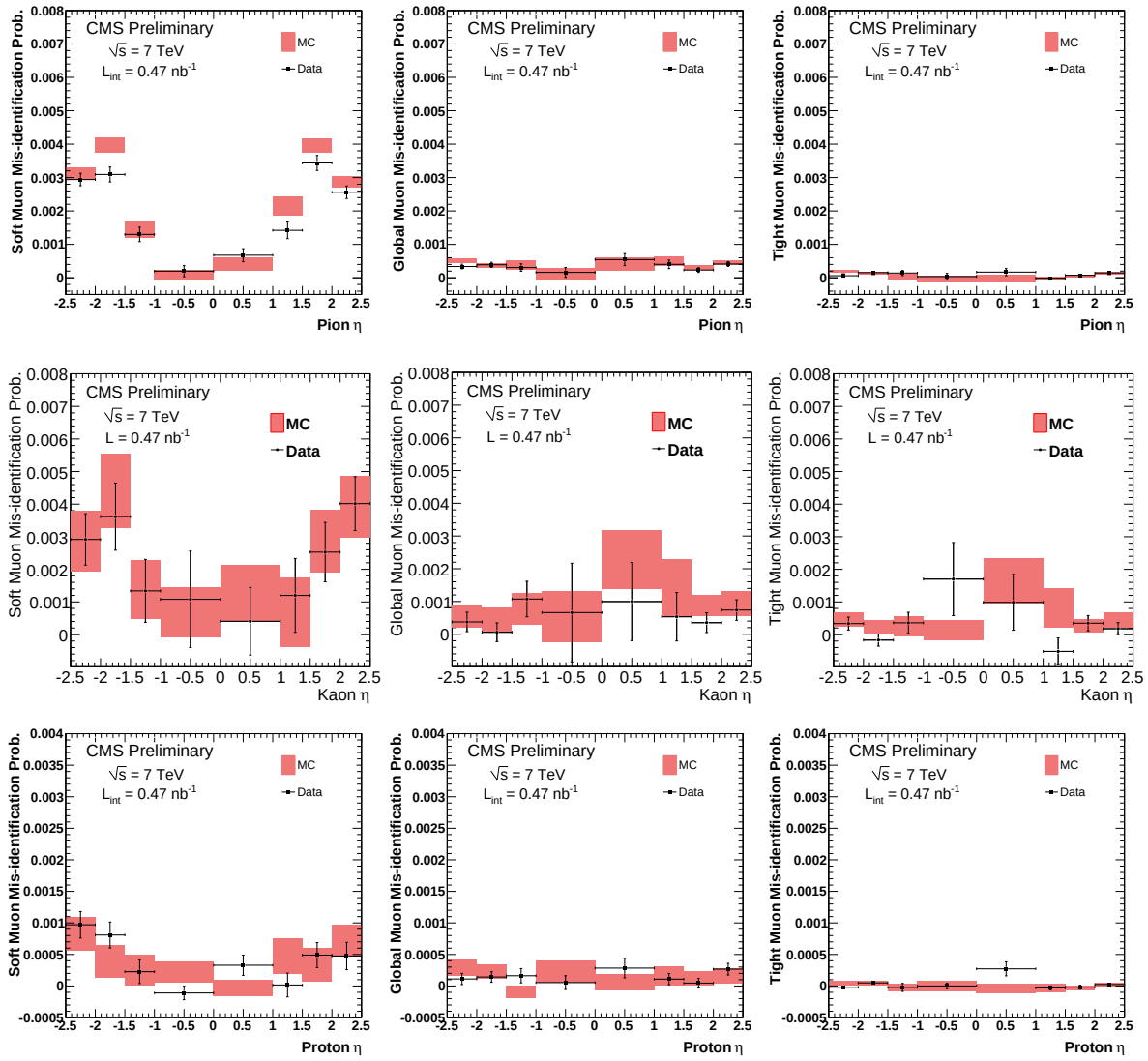

Figure 8: The fraction of pions (top), kaons (center) or protons (bottom) that are mis-identified as a Soft Muon (left), Global Muon (center), or Tight Muon (right), as a function of pseudo-rapidity. Only particles with $p > 3$ GeV/c are included. The uncertainties indicated by the error bars (data) and grey boxes (PYTHIA simulation) are statistical only.

this is mainly that Soft Muons require only a single muon chamber to be hit, in contrast to the global muon approach which typically requires at least two matches. Finally, for protons the probability to be reconstructed as a muon in the accessible momentum range is low, confirming that punch-through is small and that the muon identification probability for pions and kaons is dominated by decays-in-flight, in agreement with the prediction from simulation as discussed in Sections 3 and 4.

Table 3 summarizes the observed mis-identification probabilities in data and simulation.

5.3 Example of estimation of inclusive muon rates with and without isolation

In this section we study the fraction of tracker tracks in QCD events that are reconstructed and identified as a Tight Muon. This rate is meant to be used, for example, in Higgs analyses with

Table 3: Muon mis-identification probabilities for protons, pions and kaons for different muon selections. Uncertainties are statistical only.

	Soft Muon		Global Muon		Tight Muon	
($\times 10^{-4}$)	data	simulation	data	simulation	data	simulation
protons	5.3 ± 0.8	4.9 ± 0.9	1.5 ± 0.4	1.7 ± 0.6	0.17 ± 0.13	0.04 ± 0.14
pions	26 ± 1	31 ± 1	3.5 ± 0.4	4.1 ± 0.3	1.0 ± 0.2	1.0 ± 0.2
kaons	30 ± 4	31 ± 4	4.8 ± 1.4	7.8 ± 1.6	2.3 ± 1.0	4.0 ± 1.0

two muons in the final state to control the background coming from W+jets processes in which the W decays to a muon and an extra muon is identified in the event. The rate is calculated in a QCD data sample in order to be applied to a W+jets background sample from data.

While this fraction depends on the selection of the event sample, the larger number of muon candidates than that analysed in the previous section allows one to probe the relative rate of reconstructed muons up to higher momentum values. We use silicon tracker tracks up to $|\eta| < 2.4$ that satisfy the same tracker track quality cuts that are used for the Tight Muon selection: the track must have $|d_0| < 2$ mm and more than 10 silicon tracker hits.

Figure 9 shows the fraction of these tracks that are identified as a Tight Muon, as a function of p_{T} and η. The fraction is plotted without and with the additional requirement that the Tight Muon is isolated, where the definition of an isolated muon is based on the relative combined isolation:

$$\frac{Iso_{\mathrm{Tracker}} + Iso_{\mathrm{ECAL}} + Iso_{\mathrm{HCAL}}}{p_T^{\mu}} < 0.2. \tag{1}$$

For data, a dataset based on low-threshold jet trigger paths was used to select events with increased-p_{T} jet activity (compared to minimum-bias events). W and Z candidate events, identified as described in Ref. [11], were removed. The simulation consists of QCD events with a

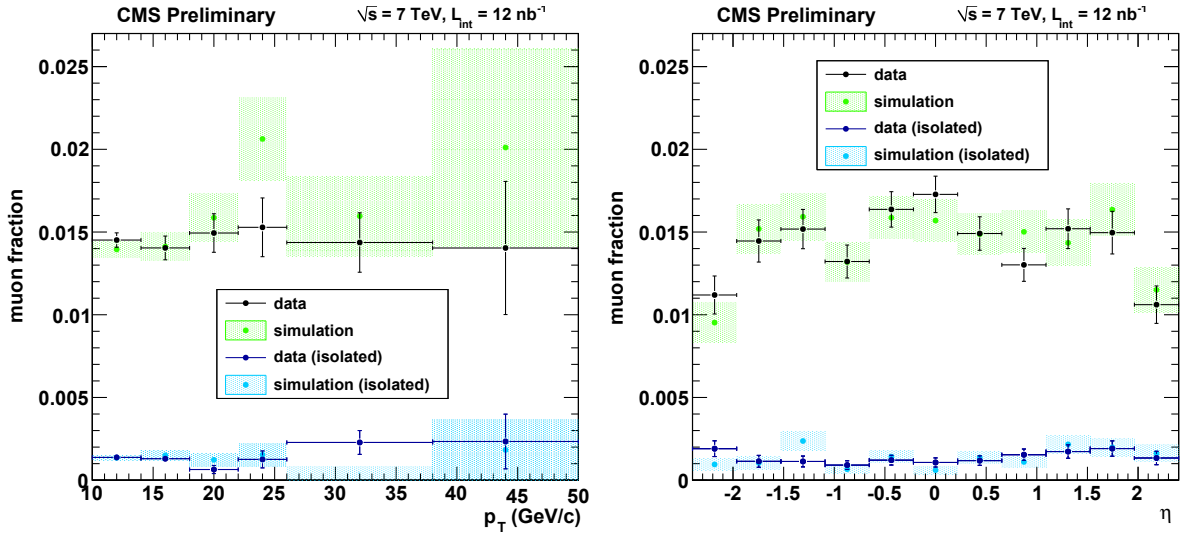

Figure 9: Fraction of silicon tracker tracks identified as Tight Muons, as a function of track p_{T} (left) and pseudo-rapidity (right), in an inclusive sample of QCD events. The effect of applying an isolation requirement is shown as well.

p_T of the partons from the hard scattering process, $\hat{p}_{\mathrm{T}}$, above 15 GeV/c.

Without isolation the overall fraction is 0.016 ± 0.003 (stat. only), while the isolation requirement reduces the fraction by another factor of ten to 0.0015 ± 0.0002 (stat. only). Both values are well reproduced by simulation. The observed fraction is higher than the exclusive muon identification probabilities for pions and kaons presented in Section 5.2, pointing at an important contribution of muons from other sources (like heavy flavour decays) in the selected event sample (cf. Section 3). Note that the inclusive muon fraction depends on the composition of the selected event sample.

5.4 Backgrounds from cosmic rays

It is possible for a cosmic muon to cross CMS in coincidence with an LHC bunch crossing. This can lead to energy deposits and a reconstructed muon track mixed with the rest of the event. However, the probability that a cosmic muon is reconstructed as a muon with a tracker track (Soft, Global or Tight Muon) is very small, and several simple reconstruction variables can be used to distinguish between muons from a collision and cosmic muons. In Fig. 10 we show a few such variables, comparing the sample of minimum bias collision data (collected using a minimum bias trigger and with a beam halo veto) with minimum bias simulation and with a cosmic-muon data sample, collected using a zero-bias trigger and selected requiring a beam halo veto and the *absence* of the minimum bias trigger. To further enhance the fraction of cosmic muon events in the latter sample, events with more than 4 reconstructed tracker tracks were rejected.

The plots are all made for Global Muons. If a cosmic muon overlaps with a collision event, and passes close enough to the center of the tracker that a Global Muon could be reconstructed, the presence of a track with almost equal p_{T} exactly opposite in direction is expected. For cosmic-ray muons, the transverse impact parameter and the muon time are not expected to peak at zero. All these features are visible in Fig. 10. The small timing offset of the peaks for collision muons is related to the current accuracy of the time pedestals of the drift tubes.

For the data recorded so far, the rate of cosmic muon coincidences of this type is very small due to the small impact parameter required, and the small time window in which the tracker reconstructs the cosmic muon track. The estimated fraction of Global Muons of this type is below 0.1%, and indeed no sign of such cosmic muons is seen in a sample of collision events, shown in the plots in Fig. 10. Note that this fraction depends on the running conditions, such as the number of proton bunches in the LHC, muon p_T thresholds, the average number of collisions per bunch crossing (pile-up), and the single-muon trigger rate.

Another way for a cosmic-ray muon to lead to a Global Muon is when a track from a collision particle is mis-matched to muon segments from the cosmic-ray muon. This is expected to happen at a higher rate, due to the much larger detector acceptance and the larger time window (several bunch crossings) over which muon hits from a cosmic muon can overlap with a collision event. On the other hand, the probability of matching is small (approx. 0.2%), and can be further reduced by about a factor of 100 with basic muon identification cuts. In addition, muon timing can discriminate between a cosmic-ray muon and a muon from the collision.

6 Muon Isolation

To measure the efficiency of an isolation requirement for prompt muons from data, we plan to exploit two distinct methods: the tag-and-probe technique described in Section 5, and the Lepton Kinematic Template Cones (LKTC) method, which is an extension of the random-cone [16]

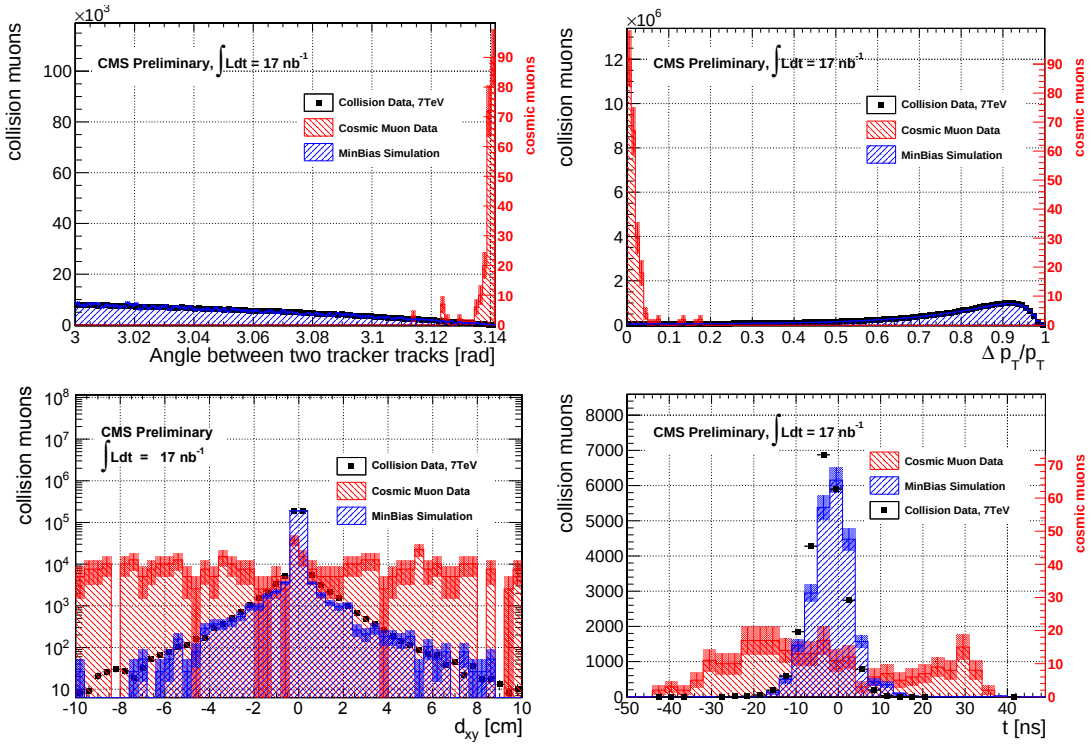

Figure 10: Comparison of variables for Global Muons in a collision-enriched sample, in a cosmics-enriched sample, and in a simulated minimum-bias sample. The relative normalization is arbitrary. The top plots show the 3D angle of Global Muons with respect to other tracks in the event (left) and the relative difference in p_{T} of Global Muons with respect to all other tracks in the event. The bottom plots show the transverse impact parameter of Global Muons (left), and their time at IP relative to the LHC clock, measured using the DT chambers.

method.

With the tag-and-probe technique, the efficiency of applying an isolation requirement can be obtained in a similar manner as other muon efficiencies, using a control sample of muons that are assumed to be isolated in an event sample of similar kinematics as the events selected for the physics analysis. A typical example would be to use $\mathrm{Z} \rightarrow \mu\mu$ events to determine the isolation efficiency for muons in $\mathrm{W} \rightarrow \mu\nu$. At present, the sample of $\mathrm{Z} \rightarrow \mu\mu$ candidates is too small to give a useful estimate of isolation efficiencies. In this section, we therefore focus on the LKTC method, and show some examples of its application to the very first collision data.

6.1 Muon isolation definitions

In the following, we use the so-called combined isolation variable, $Iso = Iso_{\mathrm{Tracker}} + Iso_{\mathrm{ECAL}} + Iso_{\mathrm{HCAL}}$, where Iso_{Tracker}, Iso_{ECAL}, and Iso_{HCAL} are respectively the sum of track p_{T}, of the transverse energy E_T in the electromagnetic calorimeter, and of the transverse energy in the hadron calorimeter, all measured in a cone of a given size (typically 0.3) in (η, ϕ)-space around the muon track direction. The track of the muon itself is excluded from the computation of Iso_{Tracker}, and the muon calorimeter deposits are excluded from the computation of Iso_{ECAL} and Iso_{HCAL} by removing calorimeter towers in a "veto cone" around the extrapolated path of the muon.

Frequently, muons originating from background processes tend to have lower p_{T} than those

from the signal. In many physics analyses, therefore, the separation between signal and background muons is improved by normalizing the isolation energy to the p_{T} of the muon, giving the relative isolation variable $RelIso = Iso/p_{\mathrm{T}}$.

The isolation properties depend on the event selection and on the type of muons considered, and will thus be different from analysis to analysis. The aim of this section is to give an estimate the efficiency for an isolation requirement for isolated muons, like those produced in Z and W decays.

6.2 Muon isolation efficiency with the Lepton Kinematic Template Cones Method

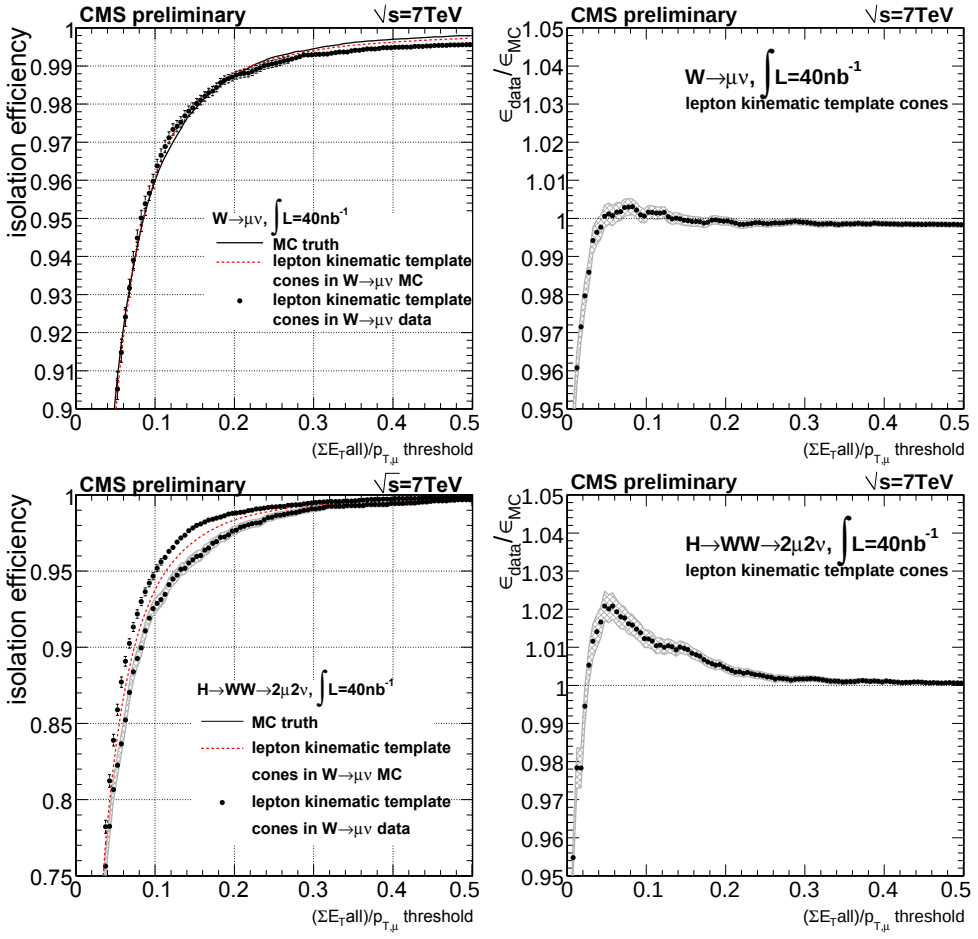

Figure 11: Isolation cut efficiency for prompt muons. Top left: efficiency (per muon) as a function of the isolation cut for muons from $W \to \mu\nu$ in simulated events, obtained from the Monte Carlo truth (solid line); isolation cut efficiency obtained by applying the LKTC method for $W \to \mu\nu$ events to simulated $W \to \mu\nu$ events (dashed line), and to candidate $W \to \mu\nu$ events in data (markers). Top right: the ratio of the efficiencies measured in data and simulation using the LKTC method. Bottom: Same set of plots, but using the LKTC method on candidate $W \to \mu\nu$ events to estimate the isolation cut efficiency (per event) in $H \to WW \to 2\mu 2\nu$ events. The grey band in the bottom left plot indicates the statistical uncertainty on the simulation truth values.

The essence of the random-cone and LKTC methods is to choose pre-defined directions in events with a similar underlying event as the signal of interest, and study energy flow around these directions. Isolation variables are defined as if these directions represent signal leptons,

so that the fraction of trials passing a given isolation cut gives the efficiency of that cut. In the definition of isolation variables, the contribution of reconstructed muons that may be present in the event is excluded.

In the random-cone method the directions are random, while in the LKTC method they are given by the directions of muons from a simulated sample of a studied signal, for example $W \to \mu\nu$, $Z \to \mu\mu$, $H \to WW \to 2\mu 2\nu$, or $ZZ \to 4\mu$. Templates allow to take into account correlations between multiple leptons in an event and include muon p_T information, so they are suitable to study relative isolation variables as well.

Figure 11 (top) shows that the isolation efficiency obtained with the LKTC method applied to $W \to \mu\nu$ simulated events [11] reproduces well the 'true' isolation efficiency for muons in $W \to \mu\nu$ simulation, as determined from the Monte Carlo truth. In data we applied the LKTC method to the sample of selected $W \to \mu\nu$ candidates (currently, 114 events [11]). The ratio of efficiencies in data to simulation is also reported, showing a good agreement. In the region of interest the difference is 1% or less. At the cut value used in the $W \to \mu\nu$ analysis (0.15) [11], the ratio is 0.9995 ± 0.0010 (stat. only).

Using the LKTC technique we can also predict the isolation efficiency for analyses with multiple (isolated) muons, where typically the isolation of the least isolated muon is used in the selection. Figure 11 (bottom) shows the efficiency of requiring both muons to be isolated in $H \to WW \to 2\mu 2\nu$, which is one of the earliest and most prominent SM Higgs analysis channels. The simulated sample used in this case is generated with PYTHIA, with $m_H = 160\ \mathrm{GeV}/c^2$. In the region of interest, agreement within 1-2% is observed.

7 Muon Trigger Performance

The CMS experiment uses a two-level trigger system. The first level is hardware-based and is called the "Level-1 Trigger" (L1) while the second level is software-based and is called the "High-Level Trigger" (HLT) [7].

Internally, the HLT algorithms consist of several steps. The HLT muon trigger follows an outside-in logic. First an L1 trigger object is used as a seed to reconstruct a standalone-muon track in the muon system. A full track fit is performed, leading to an improved p_T estimate. At this point, a p_T threshold filter can be applied to the standalone (also called L2) muon. Then seeds in the silicon tracker are generated in the region around the L2 muon, and tracker tracks are reconstructed. If a successful match can be made between a tracker track and the L2 muon, a global fit combining tracker and muon hits is performed, yielding a L3 muon track on which the final p_T requirement can be applied.

In this section we report on trigger efficiency and rejection rates observed in minimum bias data, and compare to the predictions from simulation. We study the trigger efficiency using two different, complementary methods: tag-and-probe and one using single offline-reconstructed muons. The results are reported in the $|\eta| < 2.1$ region, for a trigger path with L2 and L3 thresholds of $p_T > 3\ \mathrm{GeV}/c$.

7.1 Trigger efficiencies with the tag-and-probe method

Using the tag-and-probe method described in Section 5, the trigger efficiency is determined using muons from the J/ψ resonance.

For the tag muon we use Global Muons matched to an L1 trigger object that passed the trigger criteria. To match a reconstructed tag muon to a trigger object we use the following method: L1

trigger objects are matched by position, after extrapolating a muon's tracker track to the muon system. The HLT trigger includes reconstruction of a tracker track, and in this case the HLT muon is matched to the offline-reconstructed tracker track by direction at the vertex.

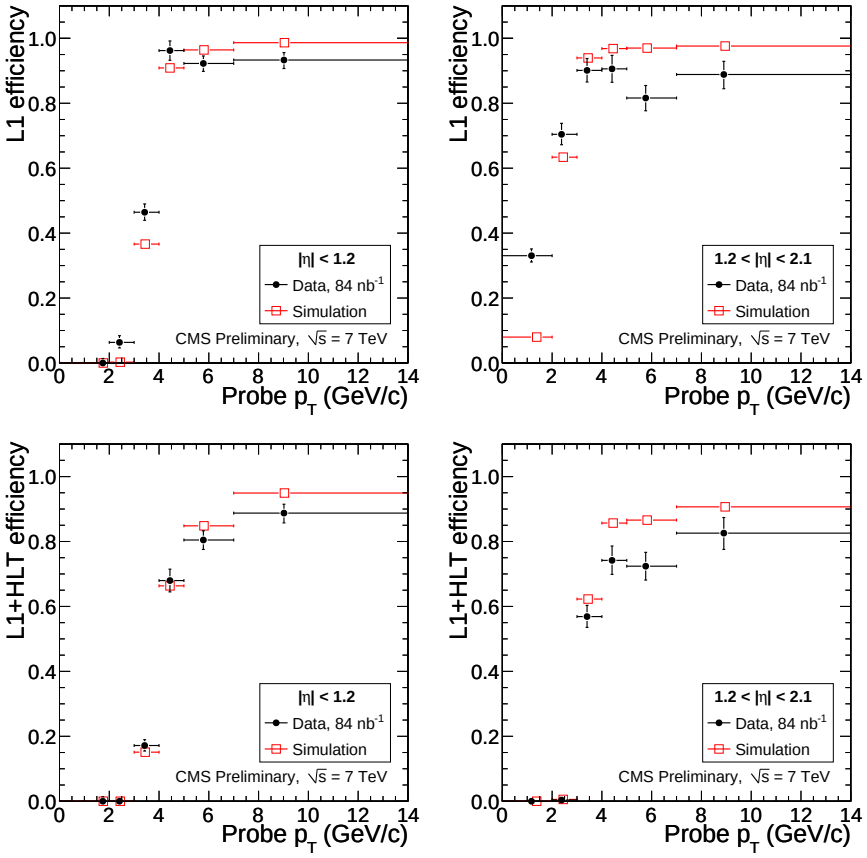

Figure 12: Tag-and-probe efficiency for data compared to simulation: the absolute trigger efficiency as a function of p_T, for L1 (top) and the combined efficiency of L1 and HLT with a threshold at 3 GeV/c (bottom) in the barrel (left) and endcap (right).

As examples, we show two types of trigger efficiencies: an absolute measurement of trigger efficiency in Fig. 12, using a tracker track with MIP signature as probe, and the efficiency with respect to a Tight Muon in Fig. 13 (top) using a Tight Muon as probe. Due to the limited statistics available, six p_T bins and two pseudo-rapidity bins are used (barrel and endcap with the boundary at $|\eta| = 1.2$). The L2 and L3 steps of the HLT trigger include a requirement of $p_T > 3$ GeV/c. While the general shape of the trigger turn-on curves agrees well between data and simulation, the plots show that the efficiency plateau at $p_T > 5$ GeV/c in data is currently a few percent lower than the expected efficiency of about 90% in the endcap and 95% in the barrel. This is mainly related to time synchronization of the muon detector at start-up. The higher L1 efficiency in the endcap at low p_T in Fig. 12 is due to special CSC trigger settings at start-up, which are designed to trigger on single muon segments to ensure the highest possible efficiency for low-p_T muons for studies of low-mass resonances like J/ψ and Y. These low-p_T muons are removed by the 3 GeV/c threshold applied in the example (L1+HLT) trigger path shown in Fig. 12 (bottom).

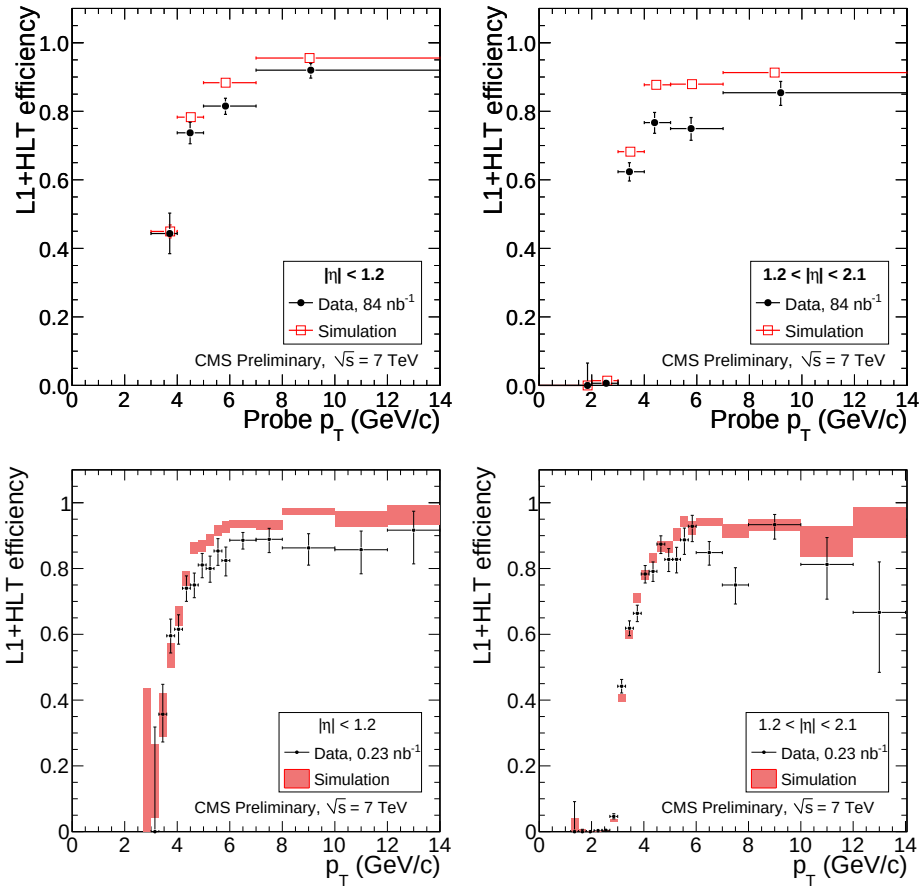

Figure 13: Same as Fig. 12, but showing the efficiency for a Tight Muon to fire the trigger. The combined efficiency of L1 and HLT with a threshold at 3 GeV/c is shown in the barrel (left) and endcap (right), using the tag-and-probe method (top) and the one using single muons (bottom).

7.2 Trigger efficiencies with respect to offline-reconstructed muons

While the tag-and-probe technique using a physics resonance allows one to determine minimally-biased trigger efficiencies for prompt signal muons, the statistical precision is limited by the number of J/ψ events. The range in which the efficiency can be probed is also restricted to the typical momentum range corresponding to the resonance.

Thus it can be useful to study the inclusive trigger efficiency for single muons, reconstructed offline with a tight muon identification selection, in a sample collected with a different trigger. In this section, we use data samples recorded with the minimum-bias trigger (to study L1 efficiencies) or a L1 muon trigger (to study HLT efficiency with respect to L1), requiring a reconstructed primary vertex.

Here we use Tight Muons as a probe. The disadvantage is that in this case only a relative efficiency can be studied, with respect to an object that already relies on muon system information. The measured efficiency is therefore biased towards high values. An additional difference with respect to the efficiency measured with the tag-and-probe technique stems from the composition of the single-muon sample: as can be seen in Table 1, about half of Tight Muons are from light flavour hadrons decaying in flight, i.e., non-prompt (and not isolated). Hence, the goal of this study is not to obtain the true, unbiased values of trigger efficiencies but to explore

differences between measured efficiency values and corresponding Monte Carlo expectations.

Using this approach, the efficiency of the different levels of the muon trigger given the presence of a Tight Muon is shown in Figs. 13 (bottom) and 14 in data and simulation. The agreement between data and simulation is at the level of 10%. The shape of the turn-on curves is well reproduced.

Several features are visible in the early data. In the endcap, the L1 efficiency in data is higher than in the simulation at low p_T. This is due to special CSC trigger settings discussed in Section 7.1. The L2 efficiency in data agrees very well with that in the simulation, both in the barrel and in the endcap. The overall L1+HLT efficiency for a given trigger path in the endcap is 5-10% lower than expected. In the barrel muon system, the L1 efficiency is about 5% lower than expected because of preliminary detector time synchronization. An additional 5% is missing in the L3 step, leading to an overall trigger efficiency in the barrel that is lower by about 10%.

During physics data-taking the thresholds are chosen such that the highest possible efficiency is obtained for signal events, while keeping the trigger rates at L1 and HLT within acceptable bandwidth. For electroweak analyses [11], currently the trigger path with a L3 threshold of 9 GeV/c is used. The lowest unprescaled single muon trigger currently has a L3 threshold of 5 GeV/c.

7.3 Trigger rejection rates

The main task of the trigger is to reduce the rate of events to be recorded, while keeping high efficiency for the physics signal events that are to be studied. Two previous sections focused on the efficiency for prompt muons to pass the trigger. In this section we discuss what fraction of minimum bias events are rejected both as a function of trigger p_T threshold at L1 and after the full HLT path, and compare to the prediction from minimum bias simulation.

The resulting rates are shown in Fig. 15. As discussed in Section 7.1, in the first runs at 7 TeV the CSC L1 trigger has been operated with special settings to ensure the highest possible efficiency for low-p_T muons in the endcaps for studies of low-mass resonances like J/ψ and Y. This leads to a better efficiency, but also less rejection. This difference is clearly visible when comparing to the emulated trigger in the simulation as in Fig. 15 (right), which corresponds to the standard trigger settings. In the central barrel region ($|\eta| < 0.8$), where CSCs are not present, the agreement at L1 is much better, as shown in Fig. 15 (left).

Both in the barrel and the endcap regions, the rate of events after the full HLT path agrees nicely with the prediction from the emulated performance in simulation. The missing rejection at L1 in the CSCs is fully recovered in the HLT. Around the threshold values for nominal low-luminosity LHC running (7 GeV/c at L1 and 16 GeV/c at L3 [17]), the agreement is very good.

The current level of agreement between the L1 and HLT trigger performance in data and the trigger emulation in simulated events is already quite good. To reproduce the trigger rate accurately, the simulation must reproduce the correct sample composition, the correct trigger efficiency, and also correctly describe the resolution for muons from different sources including the resolution tails. The results suggest that the trigger simulation will be a useful tool to predict muon trigger rates, and promise a performance of the CMS muon trigger system close to the design expectation.

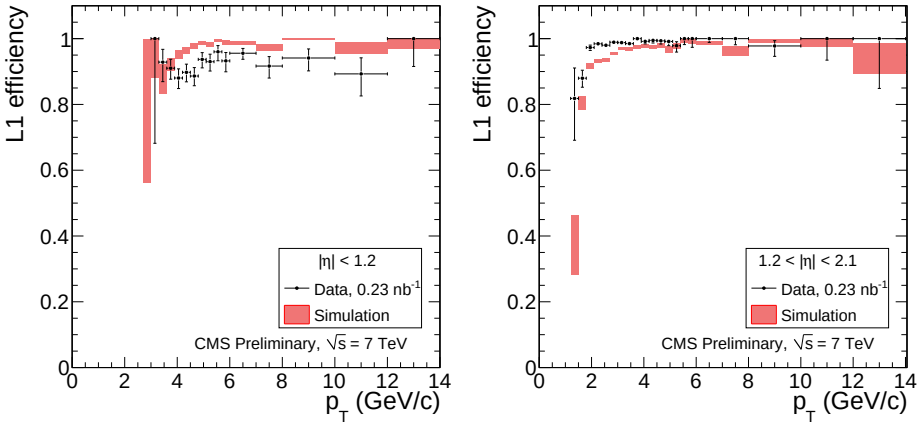

(a)

(b)

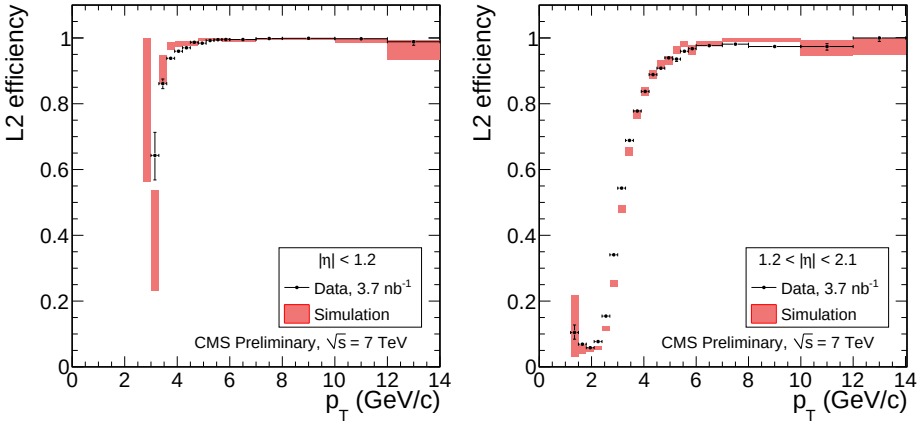

(c)

(d)

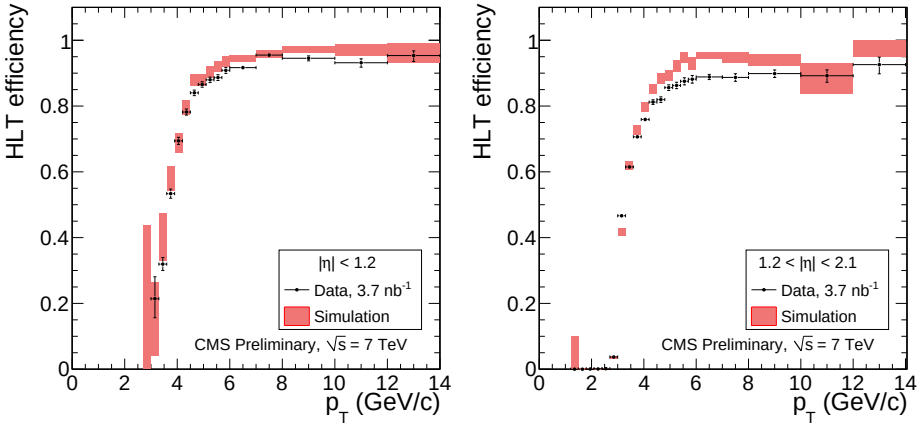

(e)

(f)

Figure 14: Single-muon trigger efficiencies for Tight Muons (without p_{T} >3 GeV/c requirement), as a function of the Tight Muon p_{T}, in the barrel (left) and endcap (right). The following efficiencies are shown: a) and b) the L1 trigger, c) and d) L2 with p_{T} threshold at 3 GeV/c with respect to L1, and e) and f) HLT with p_{T} threshold of 3 GeV/c with respect to L1. A few additional plots are shown in the Appendix.

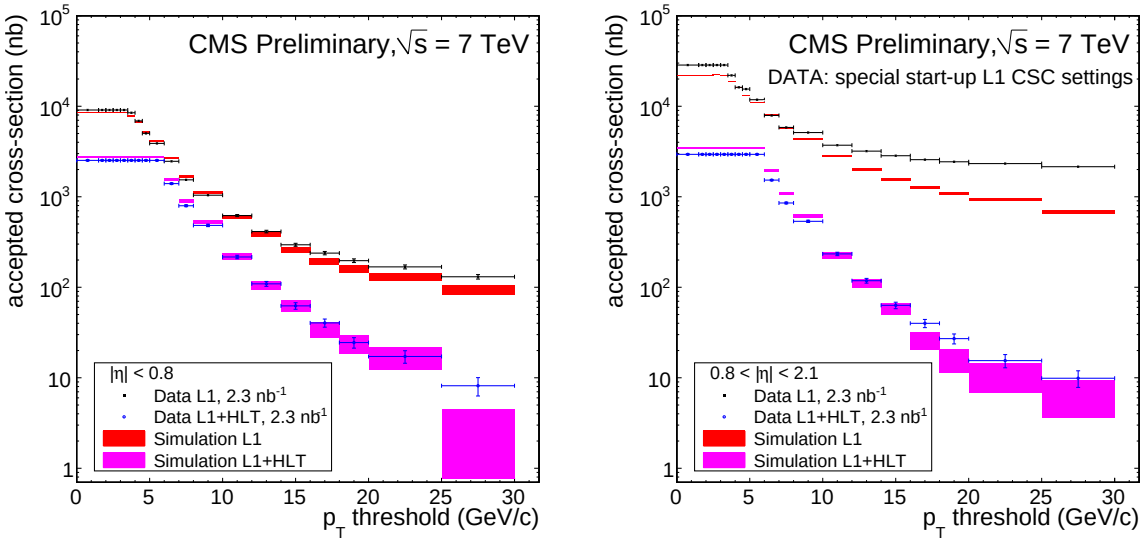

Figure 15: The accepted cross-section of events is shown as a function of trigger p_{T} threshold for the actual L1 and HLT trigger objects processed online in data, compared to the emulated L1 and HLT trigger in simulation, for the regions of $|\eta| < 0.8$ (left) and $0.8 < |\eta| < 2.1$ (right). In the data, special trigger settings were used in the endcaps, leading to a visible difference compared to the standard trigger emulation in simulation.

8 Conclusions

For the first time we report on the performance of CMS muon trigger, reconstruction and identification for muons in LHC proton-proton collisions.

With the integrated luminosity of the LHC data analyzed for this note (up to 84 nb^{-1}), most of the results are restricted to the low-momentum region. This is however an excellent opportunity to study inclusive trigger and reconstruction rates in minimum bias events, which will form an important background for physics analyses in the near future.

Several data-driven methods have been presented that allow to determine muon performance in data and compare to Monte Carlo simulation.

Good performance has been observed, close to design expectation, and the simulation has been found to reproduce well the efficiency for muons to be detected, as well as background rates for other particles to be reconstructed as muons. Trigger efficiencies and (L1+HLT) rejection rates generally agree well with the expectations.

References

[1] CMS Collaboration, "The CMS Experiment at the CERN LHC", *JINST* **3** (2008) S08004. doi:10.1088/1748-0221/3/08/S08004.

[2] CMS Collaboration, "Commissioning of the CMS experiment and the cosmic run at four tesla", *JINST* **5** (2010) T03001. doi:10.1088/1748-0221/5/03/T03001.

[3] CMS Collaboration, "Performance of CMS muon reconstruction in cosmic-ray events", *JINST* **5** (2010) T03022. doi:10.1088/1748-0221/5/03/T03022.

[4] J. Evans and P. Bryant, "LHC Machine", *JINST* **3** (2008) S08001. doi:10.1088/1748-0221/3/08/S08001.

[5] CMS Collaboration, "Measurement of Momentum Scale and Resolution using Low-mass Resonances and Cosmic-Ray Muons", *CMS PAS* **TRK-10-004** (2010).

[6] CMS Collaboration, "CMS Muon Technical Design Report", *CERN/LHCC* **1997-032** (1997).

[7] CMS Collaboration, "CMS Data Acquisition and High-Level Trigger Technical Design Report", *CERN/LHCC* **2002-026** (2002).

[8] CMS Collaboration, "CMS Physics TDR: Volume 1, Detector Performance and Software", *CERN/LHCC 2006-001* (2006).

[9] CMS Collaboration, "Measurement of Tracking Efficiency", *CMS PAS* **TRK-10-002** (2010).

[10] CMS Collaboration, "Inclusive total and differential production cross sections of J/ψ and b-hadron production in pp collisions at $\sqrt{s} = 7$ TeV", *CMS PAS* **BPH-10-002** (2010).

[11] CMS Collaboration, "Measurements of Inclusive W and Z Cross Sections in pp Collisions at $\sqrt{s} = 7$ TeV", *CMS PAS* **EWK-10-002** (2010).

[12] T. Sjöstrand, L. Lönnblad and S. Mrenna, "PYTHIA 6.2: Physics and manual", arXiv:hep-ph/0108264.

[13] CMS Collaboration, "Measurement of CMS Luminosity", *CMS PAS* **EWK-10-004** (2010).

[14] The CMS Collaboration, "CMS Muon Performance Results Web Page", **https://twiki.cern.ch/twiki/bin/view/CMSPublic/PhysicsResultsMUO**.

[15] CMS Collaboration, "Tracking and Vertexing Results from First Collisions", *CMS PAS* **TRK-10-001** (2010).

[16] S. Abdullin et al., "Sensitivity of the Muon Isolation Cut Efficiency to the Underlying Event Uncertainties", *CMS Note* **2006/033** (2006).

[17] CMS Collaboration, "CMS High Level Trigger", *CERN/LHCC 2007-021* **LHCC-G-134** (2007).

A Interesting event displays

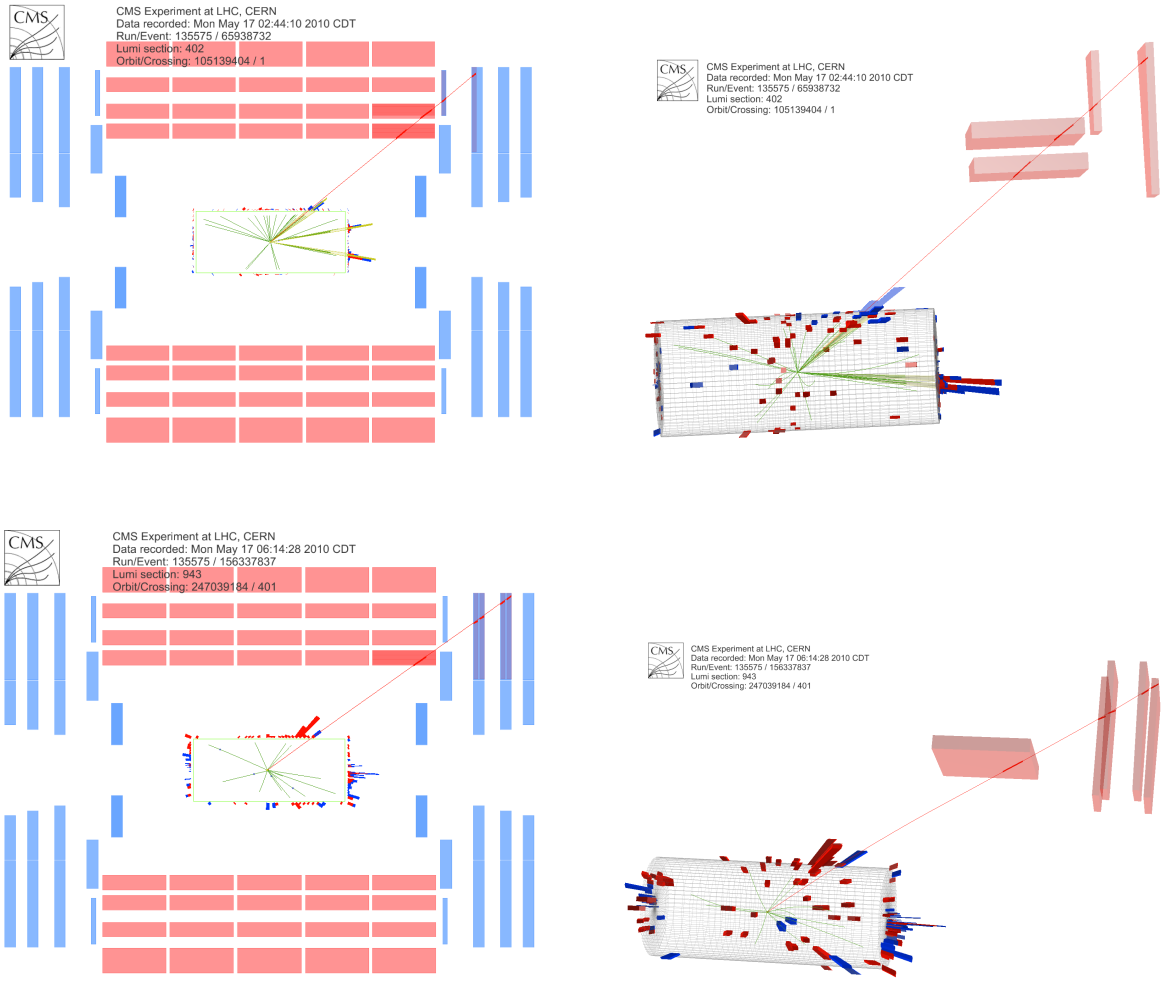

Figure 16: (Color online.) Two events from run 135575 with a muon in the overlap region. A Rho-Z projection is shown on the left, and 3D view on the right. DT and CSC segments are indicated by red stubs (best visible in the 3D view). Energy deposits in the electromagnetic (red) and hadronic (blue) calorimeters are shown as well. The first event has a muon (in a jet) that is classified as both a Soft Muon and a Global Muon, with 4 segments matched and $p_{\mathrm{T}} = 12.2$ GeV/c. The muon in the second event is also classified as both a Soft Muon and a Global Muon, has $p_{\mathrm{T}} = 7.4$ GeV/c and passes through a region where CSC chambers overlap, yielding 5 matched segments.

B Additional trigger efficiency plots

In the HLT trigger path considered in this note, the L2 p_{T} threshold is 3 GeV/c. The wider momentum resolution at L2 thus determines the shape of the trigger turn-on curves when at L3 the same 3 GeV/c is used, as in Fig. 14. To appreciate the good resolution of the tracker tracks used at L3, Fig. 17 shows in addition the efficiency when the L3 threshold is increased to 7 GeV/c. As expected, the turn-on curve has a much sharper edge, reflecting the improved momentum resolution at L3.

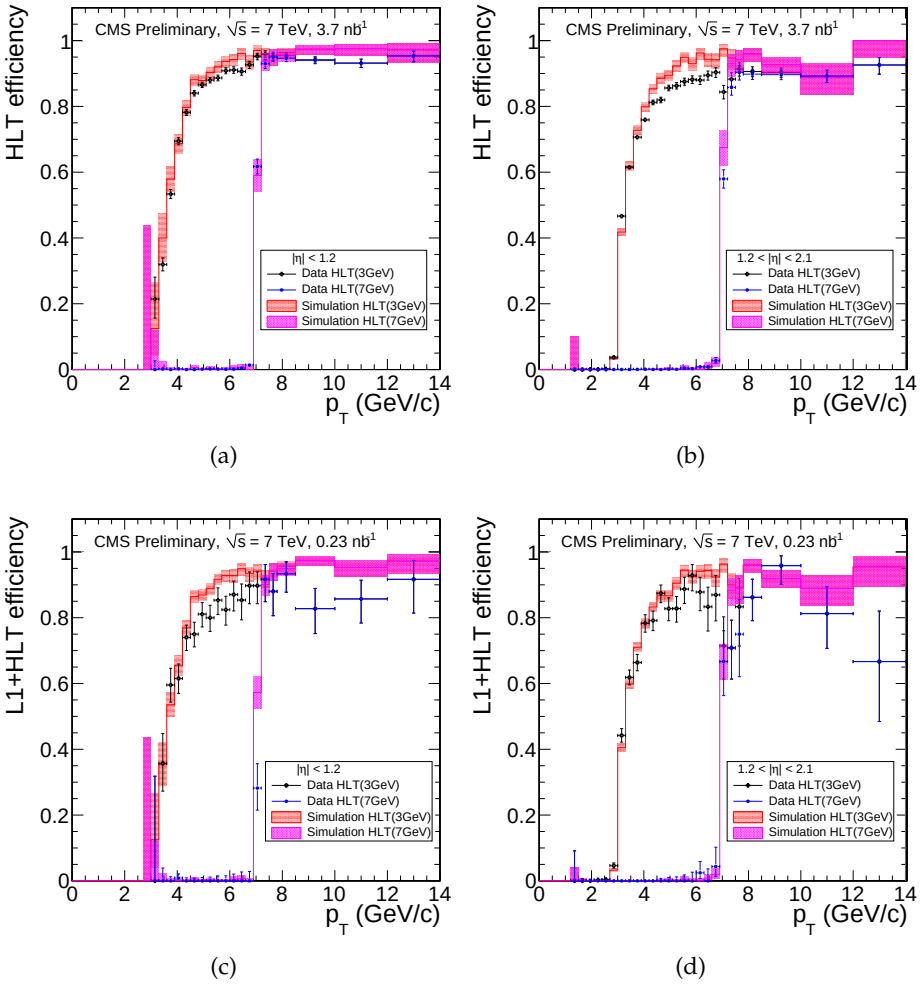

Figure 17: Single-muon trigger efficiencies for Tight Muons, as a function of the Tight Muon p_{T}, in the barrel (left) and endcap (right). In these plots, the L1 and L2 p_{T} thresholds are set to 0 GeV/c and 3 GeV/c, respectively, and the efficiencies are shown for two choices of the L3 p_{T} threshold, 3 GeV/c and 7 GeV/c. The sharpness of the trigger turn-on curve for 7 GeV/c threshold reflects the good resolution of the HLT trigger due to the use of a silicon tracker track at L3. Panels a) and b) show the HLT efficiencies with respect to L1 and correspond to e) and f) in Fig. 14; c) and d) show the combined L1+HLT efficiencies, corresponding to c) and d) in Fig. 13.